Available online at www.sciencedirect.com
ScienceDirect
Polymer 47 (2006) 6472–6480
polymer
www.elsevier.com/locate/polymer

Numerical simulation of substrate effects on spinodal decomposition in polymer binary mixture: Effects of the surface potential

Li-Tang Yan, Xu-Ming Xie*

Advanced Materials Laboratory, Department of Chemical Engineering, Institute of Polymer Science and Engineering, Tsinghua University, Beijing 100084, PR China

Received 6 April 2006; received in revised form 15 June 2006; accepted 1 July 2006
Available online 28 July 2006

Abstract

The surface-directed spinodal decomposition (SDSD) of polymer binary mixture with different values of surface potential is numerically simulated in three-dimension (3D) by cell dynamic systems (CDS). Furthermore, the growth laws of the wetting layer are theoretically analyzed by the current equation and the dynamical scaling. The results show that the thickness of the wetting layer increases with the increasing surface potential. The crossover, which is later for larger values of surface potential, appears in the evolution curve of the wetting layer. Before the crossover, the growth law is the surface potential dependant growth law. Subsequently, the growth law is the typical Lifshitz–Slyozov (LS) growth law. The results indicate that the surface potential can result in the mutual transformation between completely wetting and partially wetting for the substrate interface. It can be found that the higher surface potential leads to the faster and stronger transmission of the effect of the substrate on the spinodal decomposition in the bulk.

Keywords: Substrate effect spinodal decomposition; Cell dynamic system; Simulation

1. Introduction

The SDSD has been paid much attention in recent years since it is of great importance in both the theoretical study and the industrial application [1–3]. In this case, the substrate interface is completely or partially wetted by the preferred component and becomes the origin of anisotropic spinodal decomposition waves, which propagate into the bulk perpendicular to the substrate surface [2,3].

This problem is also of great experimental interest, and was first studied by Jones et al. [3] in the context of phase separating polymer mixtures in a ''semi-infinite'' geometry. These authors examined laterally averaged composition profiles as a function of distance from the substrate surface. They found that the phase morphology near the substrate is time dependant and propagates into the bulk. There have been many subsequent experiments on this problem [4–23]. For example, Guenoun et al. [4] and others [5–7] found that the phase growth parallel to the substrate surface was suppressed and, if a power law fit was attempted, it would show a crossover of the exponent from 1/3 to 1/2. It is of even greater interest to study the opposite limit of a strong surface field [8,9]. In this case, there is rapid formation of a multi-cross-sectioned structure near the substrate surface. Recent interest has also focused on SDSD in other contexts, such as SDSD on patterned substrates [10,11], spinodal dewetting [12,13] and so on [14–23].

Along with the experimental observation, computer simulation plays an increasingly important role in understanding the mechanism of morphological changes in binary mixture [24–40]. The first phenomenological model of SDSD was proposed by Puri and Binder [24]. This and similar models have been studied analytically and numerically by various authors [25–29]. The SDSD of binary mixture has also been extensively investigated by cell dynamic system (CDS) [30–32], microscopic models (e.g. the spin-exchange Ising model) [33,34]

* Corresponding author. Tel.: +86 10 6277 3607.
E-mail address: xxm-dce@mail.tsinghua.edu.cn (X.-M. Xie).

0032-3861/$ - see front matter © 2006 Elsevier Ltd. All rights reserved.
doi:10.1016/j.polymer.2006.07.008

and Monte Carlo simulation [35]. These modelings have also been extended naturally to the problem of phase separation in a confined geometry (e.g. thin film), where novel physical effects arise due to the interplay for SDSD waves arising from different boundaries. For instance, Puri, Binder, and Frisch have studied domain growth adjacent to the wetting layer for both a critical quench [25,26] and an off-critical quench [27,28] with a variety of surface potentials. Marko [30] also considered SDSD in 2D with both short-range and long-range surface forces by CDS. Employing Monte Carlo simulation, Rysz [35] studied the SDSD in thin polymer blend film.

In our previous study [32], the morphology and dynamics of the polymer binary mixture for SDSD in 3D have been studied by CDS, focusing on the dynamic behavior of parallel cross-sections. As our concern was the dynamical behavior of the parallel cross-section, the simulations were done with a certain surface potential. It should be pointed out that the growth mechanism of the wetting layer has an important correlation with the surface potential [2,9]. So, it is important to study the effect of the varying surface potential by numerical simulation.

In the present paper, the SDSD with different values of surface potential will be numerically simulated in 3D by CDS. Our main purposes are to give the detail relationship between the surface interaction and the wetting layers, and to exhibit dynamical behaviors of the parallel and perpendicular cross-sections with different values of surface potential.

2. Models and algorithm

The dynamics and morphology evolution are described by the CHC equation for diffusive field, which can be written as [41]

$$\frac{\partial\psi(r,t)}{\partial t} = M\nabla^2\frac{\delta F(\psi(r,t))}{\delta\psi(r,t)} + \eta(r,t) \tag{1}$$

Here $\psi(r,t) = \phi(A) - \phi(B)$ is the order parameter of the system at point r at time t. $\phi(A)$ and $\phi(B)$ are, respectively, the local volume fraction of components A and B. We have used the fact that $\psi(r,t)$ is a conserved order parameter. M is a phenomenological parameter. $F(\psi(r,t))$ is usually the coarse-grained free-energy function. In the present study, we have chosen z axis as the direction of the surface effect and consider a substrate surface located at $z = 1$. Thus, for the surface-directed spinodal decomposition, $F(\psi(r,t))$ can be defined as [30]

$$\frac{F(\psi(r,t))}{k_BT} = \int \mathrm{d}r\left[\frac{\varepsilon}{2}\psi(r,t)^2 + \frac{u}{4}\psi(r,t)^4 + \frac{c}{2}(\nabla\psi(r,t))^2 - \sum_n \frac{1}{n}\left[S^{(n)}(z)\right]\psi(r,t)^n\right] \tag{2}$$

where $S(z)$ describes the surface fields and T is the temperature. ε, u and c are phenomena parameters and can be related to the molecular characteristics [42]. This model with $n = 1, 2$ surface potentials is the basic model used to study equilibrium wetting phenomena [30,43]. The case with $n = 1$, which considers the difference between the interfacial tensions of the two pure components with the surface, indicates an integrated substrate potential. However, the $n = 2$ fields oppose the formation of either ordered phase due to the smaller coordination number of molecules at the surface compared to those in the bulk [30]. $n = 1$ is set in the simulation that indicates an integrated substrate potential in the present paper. And $\eta(r,t)$ is a Gaussian white noise, representing the thermal fluctuation, with mean zero and correlation

$$\langle\eta(r,t)\eta(r',t)\rangle = -2k_BTM\nabla^2\delta(r-r')\delta(t-t') \tag{3}$$

where T is the temperature of the fluid and $\langle\ldots\rangle$ denotes the ensemble average. As a minimal model, any hydrodynamic effects and possible nonlocality in the mobility coefficient can be ignored [44,45]. For simplicity, the thermal noise is also neglected in this simulation. But we must point out that the thermal noise has an effect on the final phase morphology to a certain extent. The effect of noise has been discussed in the other work [46]. The driving force of the phase separation is due to the chemical potential $\mu(r,t)$ with $\mu(r,t) = \delta F(\psi(r,t))/\delta\psi(r,t)$. According to Eq. (2), the chemical potential has the form

$$\frac{\mu(r,t)}{k_BT} = \varepsilon\psi(r,t) + u\psi(r,t)^3 - c\nabla^2\psi(r,t) - \sum_n S^{(n)}(z)\psi^{n-1} \tag{4}$$

with the substitution of the dimensionless variables

$$r\to r/\sqrt{c/\varepsilon},\ \tau\to t/\left(c/M\varepsilon^2k_BT\right),\ \psi(r,\tau)\to\psi(r,t)/\sqrt{\varepsilon/u} \tag{5}$$

Then, Eq. (2) becomes

$$\frac{\partial\psi(r,\tau)}{\partial t} = \nabla^2\left[\psi + \psi^3 - \nabla^2\psi - \sum_n S^{(n)}(z)\psi^{n-1}\right] \tag{6}$$

The boundary conditions at the substrate can be defined as

$$\nabla\mu(r,\tau) = 0|_{Z=1}$$

$$\nabla\psi + \sum_n S^{(n)}\psi^{n-1} = 0|_{Z=1} \tag{7}$$

Eq. (4) is numerically solved by CDS proposed by Puri and Oono [47,48]. In the 3D CDS, the system is discretized on an $L_a \times L_a \times L_a$ cubic lattice. And the order parameter of each cell is defined as $\psi(r,\tau)$, where $r = (r_x, r_y, r_z)$ is the lattice position and r_x, r_y and r_z are the integers between 1 and L_a. According to CDS, the polynomial $\psi + \psi^3 - \nabla^2\psi$ is replaced by $A\tanh\psi - \psi + D[\langle\langle\psi\rangle\rangle - \psi]$, where A is a phenomenological parameter characterizing the quenching depth and D can be related to the interfacial free energy. And $\langle\langle\psi(r)\rangle\rangle$ represents the following summation of $\psi(r)$ for the nearest neighbors $(r.)$, the next-nearest neighbors $(r.r.)$, and the next-next-nearest neighbors $(r.r.r.)$

$$\langle\langle\psi(r)\rangle\rangle = B_1 \sum_{r=r.} \psi(r) + B_2 \sum_{r=r.r.} \psi(r) + B_3 \sum_{r=r.r.r.} \psi(r) \tag{8}$$

where B_1, B_2, and B_3 are 6/80, 3/80 and 1/80, respectively for the 3D system. Considering only a long-range "van der Waals" potential, the surface effect can be transformed into $S(Z) = Ha(1 + (Z-1)^{\Theta})^{-1}$, where Ha measures the strength of the surface potential and $\Theta = 3$ specifies its range [30]. In this case, the sum $\sum_Z S(Z) \approx 1$, and so Ha is of order of the total integrated surface potential. Then, Eq. (6) is transformed to the following difference equation:

$$\psi(r, \tau + 1) = \psi(r, \tau) - R(\langle\langle I(r, \tau)\rangle\rangle - I(r, \tau)) \tag{9}$$

with

$$I(r, \tau) = A \tanh \psi - \psi + D[\langle\langle\psi\rangle\rangle - \psi] + S(Z) \tag{10}$$

Discretizing the boundary conditions, i.e. Eq. (7), at substrate surface ($z = 1$) gives $\psi(-1, \tau) = \psi(1, \tau)$ and $I(-1, \tau) = I(1, \tau)$. Furthermore, the periodic boundary conditions are used in the x and y directions and free boundary conditions are applied at the other end in the z direction.

The parameters are set $A = 1.3$, $D = 0.7$ and $R = 1$ in the present simulation, respectively. Different values of Ha were selected to investigate the effects of the surface potential. Our simulation was carried out on $L_a \times L_a \times L_a = 64 \times 64 \times 64$ 3D cubic lattice. And the dimensionless spatial increment is $\Delta x = \Delta y = \Delta z = 1$. The dimensionless time step is set as $\Delta\tau = 1$. The range of the field ψ at $\tau = 0$ is $\bar{\psi} - s \le \psi \le \bar{\psi} + s$ with the random fluctuation $s = 0.1$, where the spatial average of ψ is $\bar{\psi} = 0$. The initial conditions correspond to the case of critical quenches.

3. Results and discussions

3.1. Time evolution of simulated patterns with different surface potentials

We would first like to show how SDSD develops in 3D. Fig. 1 indicates the pattern evolution of SDSD with $Ha = 0.4$. In Fig. 1, the regions with positive order parameter (A rich phase; say, A-rich) are marked. It can be clearly seen from Fig. 1 that the wetting surface layer changes rapidly and becomes an A-rich cross-section, followed by B-rich cross-section. The longer the time, the thicker the A-rich cross-section is. Next to the B-rich cross-section, one can see a very clear two-phase structure showing a typical percolated network patterns before $\tau = 800$. However, after $\tau = 800$, the break-up of the percolated network can be found. The percolated network gradually disrupts or breaks up into many fragments. With further increasing time, the irregularly shaped fragments shrink and then reshape into many anisotropic drops and droplets. The simulation reproduces the basic features of experimental observation [14–20].

The simulated pattern evolution with $Ha = 0.02$ is shown in Fig. 2. In contrast to Fig. 1, it is found that the substrate surface is only partially wetted by component A with many holes, which is really component B, in it. And with the increasing time, the holes in the wetting layer become gradually bigger. The wetting layer coarsens and almost disappears in the later time. This demonstrates that the weaker surface potential can lead to a partially wetting surface layer. In other words, the surface potential can result in the mutual transformation between completely wetting and partially wetting for the

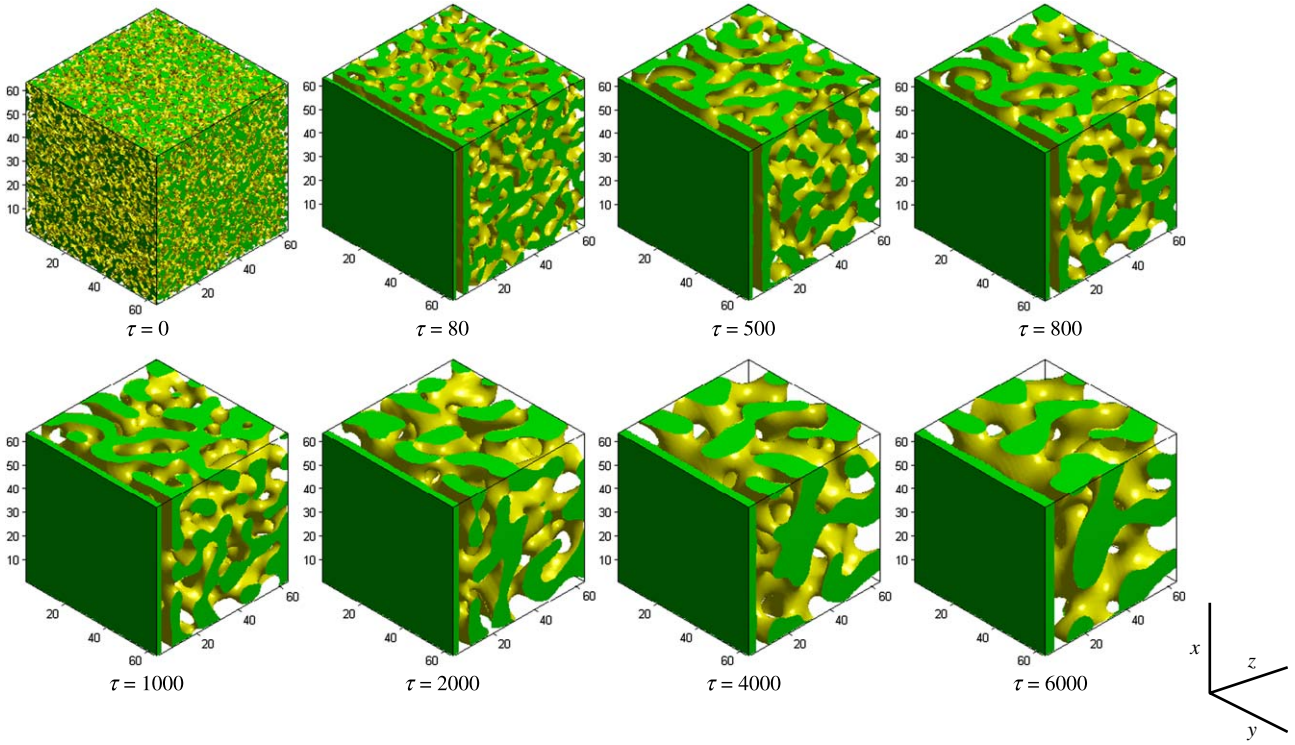

Fig. 1. Simulated pattern evolution of surface-directed spinodal decomposition in 3D with $Ha = 0.4$.

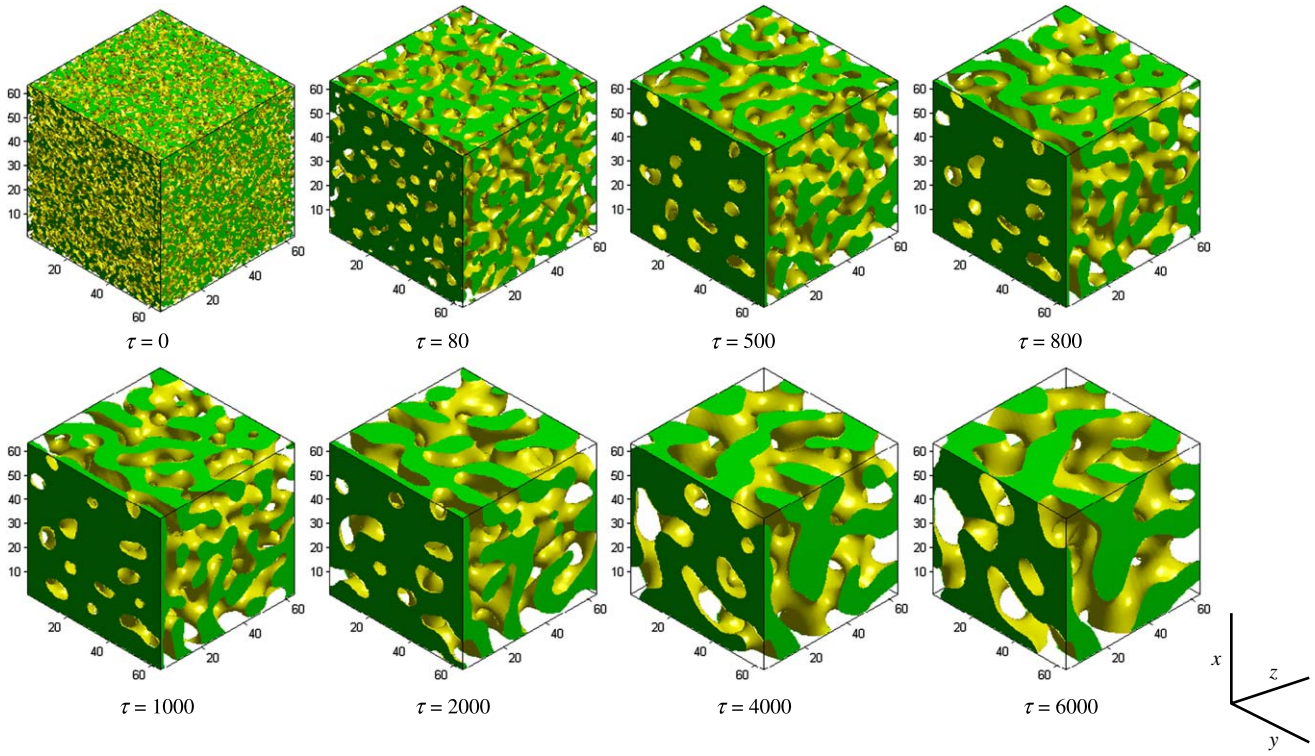

Fig. 2. Simulated pattern evolution of surface-directed spinodal decomposition in 3D with $Ha = 0.02$.

substrate interface, which is basically consistent with Marko's report [30].

3.2. Effects of the surface potential on the mechanism of the wetting layer

Fig. 3 shows the averaged profiles in the z direction for the evolution of the patterns of Fig. 1. The averaged profiles are obtained by averaging the order parameter profile $\psi(x, y, z, \tau)$ of the cross-sections along z axis as Eq. (11) with $N_{x,y} = \psi_{\mathrm{av}}(0, \tau)$ for a single run and then ensemble averaging over 50 different runs,

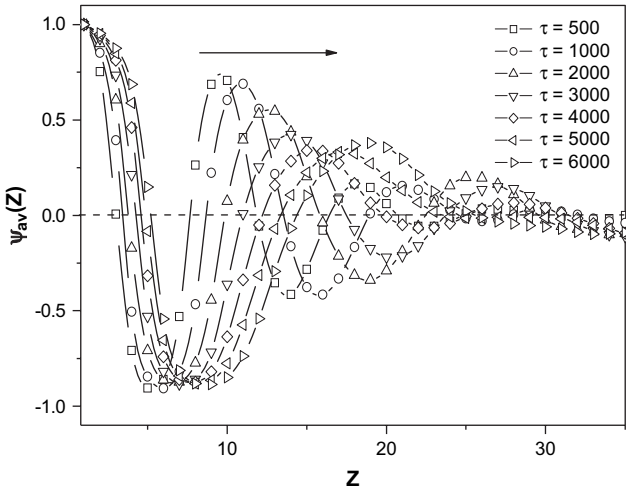

Fig. 3. The averaged profiles in the z direction at different times with $Ha = 0.4$.

$$\psi_{\mathrm{av}}(z, \tau) = \frac{1}{N_{x,y}} \sum_{x,y} \psi(x, y, z, \tau) \tag{11}$$

It is seen that the hallmark of SDSD, i.e. a profile that oscillates with a characteristic wavelength, is presented near the substrate surface, which slowly propagates out into the bulk. And the averaged profiles decay to zero in the bulk where spinodal decomposition waves are isotropic and randomly oriented. The thickness of the wetting layer can be measured by finding the Z position $R(\tau)$ of the first zero of the Z-order parameter profile.

Fig. 4 shows the evolution of $R(\tau)$ with the increasing time, τ, in the log–log scale. It can be found that the values of $R(\tau)$ increase with the increasing Ha. On the other hand, the thickness of the wetting layer for different values of Ha evolves with almost the same speed initially and then cross over to a faster growth. The crossover is later for larger values of Ha and, it is obvious that the crossover does not appear during the current time when the value of Ha is more than 0.7. Before the crossover, the growth law is $R(\tau) \propto \tau^{1/5}$, demonstrating the surface potential dependant growth law [27]. Subsequent to the crossover, the accelerated growth seems to fit a faster law with about $R(\tau) \propto \tau^{1/3}$, indicating the typical LS growth law [49].

How can one understand these results? Fig. 5 is the schematic diagram showing the enrichment of the wetting layer in side view. The preferred component, A, must feed the wetting layer due to the attraction of the substrate, and this requires diffusion through the depletion zone [30]. In this case, the wetting layer grows due to two contributions to the

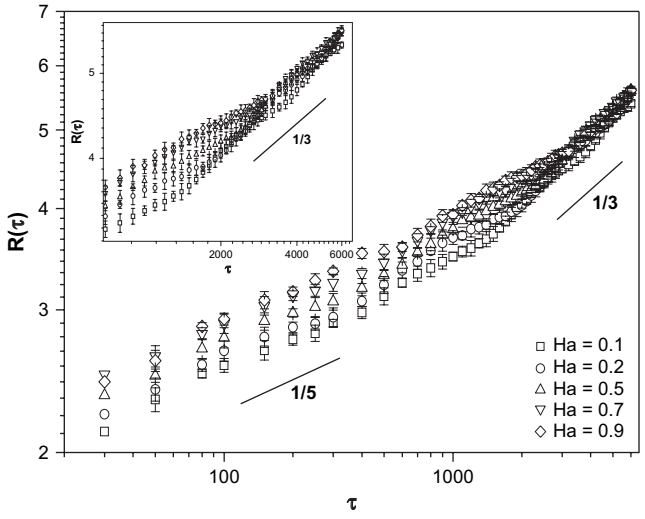

Fig. 4. The plot of the thickness of the wetting layer, $R(\tau)$, with the increasing time, τ, in the log–log scale. The inset is the data in the late stage.

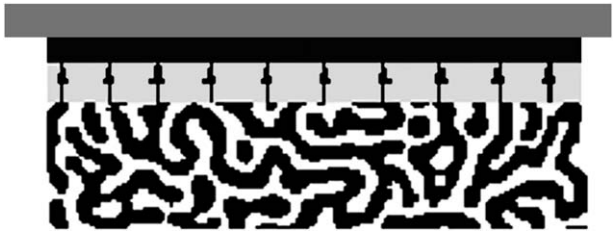

Fig. 5. The schematic diagram showing the enrichment of the wetting surface layer in side view.

chemical potential gradient (or current): (a) the surface potential gradient drives A to the wetting layer with a current $\mathrm{d}S(Z)/\mathrm{d}Z|_{Z=R}$; (b) the intrinsic chemical potential (due to local curvature) is higher on the curved surface of bulk phase than on the flat wetting layer. Synthetically considering these two contributions, the current J_Z at $Z=R$ can be estimated as follows [27,28]:

$$\frac{\mathrm{d}R}{\mathrm{d}\tau} = -J_Z \approx \frac{\Theta Ha}{R^{\Theta+1}} + \frac{\sigma}{R_0 R}\left(1+\frac{1+\bar{\psi}}{1-\bar{\psi}}\right) \tag{12}$$

where σ is the surface tension and R_0 is the bulk length scale. The bulk length scale obeys the LS growth law, i.e. $R_0(\tau) = f(\bar{\psi})(\sigma\tau)^{1/3}$, where the function $f(\bar{\psi})$ is known analytically in the limit $|\bar{\psi}|\to 1$ [50,51], and studied numerically for other values of $\bar{\psi}$ [47,48]. As R grows with time, the first term on the right-hand side of Eq. (12) is dominant at the early stage and the second term is dominant at the late stage. This yields the growth regimes as

$$R(\tau) \approx \begin{cases} [\Theta(\Theta+2)Ha]^{1/(\Theta+2)}\tau^{1/(\Theta+2)}, & \tau \le \tau_c \\ \sqrt{\dfrac{3}{f(\bar{\psi})}\dfrac{(1+\bar{\psi})}{(1-\bar{\psi})}}(\sigma\tau)^{1/3}, & \tau \ge \tau_c \end{cases} \tag{13}$$

where τ_c is the crossover time and can be obtained by equating the early-time and late-time scales as

$$\tau_c \approx [\Theta(\Theta+2)Ha]^{3/(\Theta-1)} \times \left[\frac{f(\bar{\psi})}{3}\frac{1-\bar{\psi}}{1+\bar{\psi}}\right]^{3(\Theta+2)/2(\Theta+1)} \sigma^{-[(\Theta+2)/(\Theta-1)]} \tag{14}$$

Clearly, the growth law of the wetting layer in the early stage obeys $R(\tau)\propto\tau^{1/(\Theta+2)}$, which is the surface potential dependant growth law. As $\Theta = 3$ is set in the simulation, the growth law in the present study is $R(\tau)\propto\tau^{1/5}$ in the early stage. The asymptotic growth law in the late stage is $R(\tau)\propto\tau^{1/3}$, i.e. an LS growth law. It can be found from Eq. (14) that the crossover between the potential dependant growth regime and the LS growth regime can be extremely delayed with the increasing Ha.

It has been demonstrated theoretically [52] and experimentally [4] that when there is only one relevant length scale present, or when all length scales have the same growth law, dynamical scaling should occur. Fig. 6 shows the rescaled averaged profiles in the early stage and the late stage,

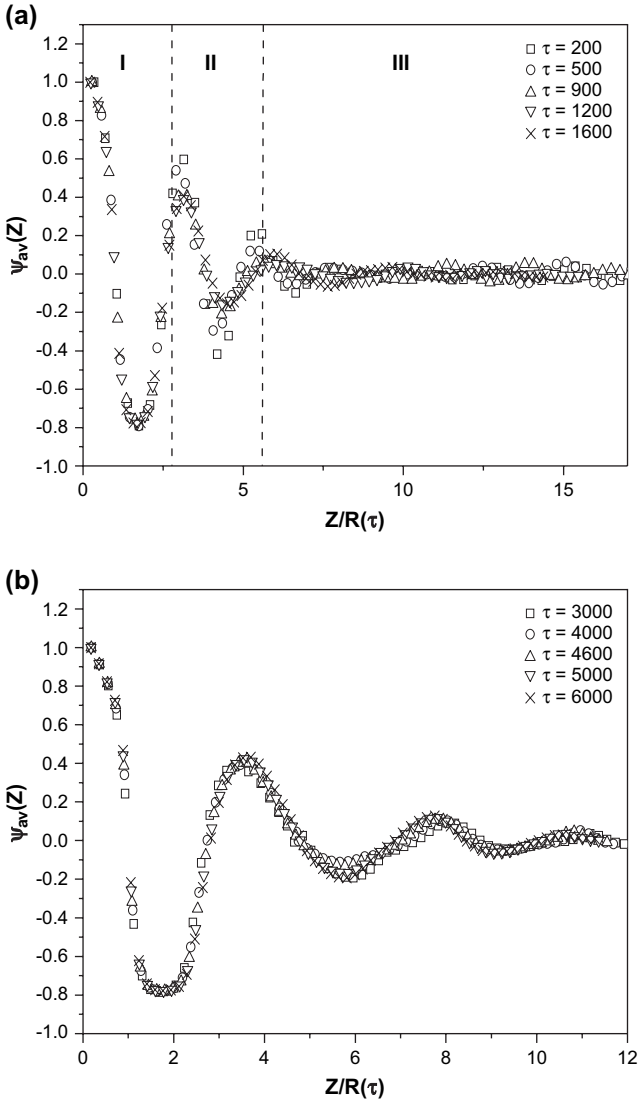

Fig. 6. The rescaled averaged profiles at different times with $Ha = 0.6$. (a) In the early stage. (b) In the late stage.

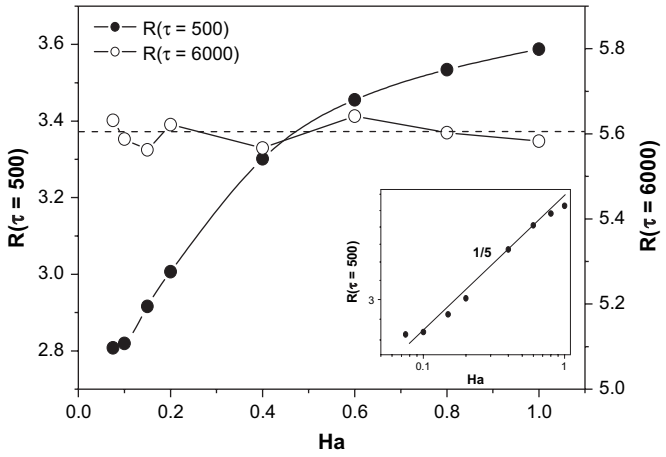

Fig. 7. Plots of the thickness of the wetting layer, R, with different values of Ha at $\tau = 500$ and $\tau = 6000$. The inset is the plot at $\tau = 500$ in the log–log scale.

respectively with $Ha = 0.6$. From Fig. 6(a), it can be found that the variation of the rescaled profiles in the early stage can be divided into three regimes. In the first and the third regimes, the profiles at different times fall on a master curve, respectively, demonstrating the dynamical scaling in these two regimes. However, there is no dynamical scaling in the second regime. As the dynamical behavior in the second regime is affected by those both in the first regime and in the third regime, these results demonstrate that the growth laws in the first and third regimes are different. According to the previous results [49], it can be known that the bulk growth law (the third regime) is LS growth law and the growth law near the substrate surface (the first regime) is surface potential dependant growth law. Fig. 6(b) shows the rescaled profiles in the late stage. It is seen that the profiles at different times fall on a master curve, indicating the same dynamical scaling and growth law in all values of Z. As a matter of fact, the growth law is the LS growth law.

From Eq. (13), it can be found that the thickness of the wetting layer, $R(\tau)$, obeys the rule of $R(\tau) \propto Ha^{1/(\Theta+2)}$ in the early stage with the increasing Ha. In the late stage, $R(\tau)$ has no relation with Ha. Fig. 7 shows the plots of the thickness of the wetting layer, R, with different values of Ha at $\tau = 500$ and $\tau = 6000$. The inset is the plot at $\tau = 500$ in the log–log scale. The figure illustrates that R increases markedly with the increasing Ha. And the rule at $\tau = 500$ is about $R \propto Ha^{1/5}$. It can also be found that the values of R with different values of Ha only fluctuate involving a certain value. All these simulated results are basically consistent with the theory analysis result as Eq. (13).

3.3. Effects of the surface potential on the evolution of the phase morphology

In order to more clearly understand the effects of the surface potential on the evolution of the phase morphology, some cross-sections perpendicular and parallel to the substrate surface with different values of Ha are investigated.

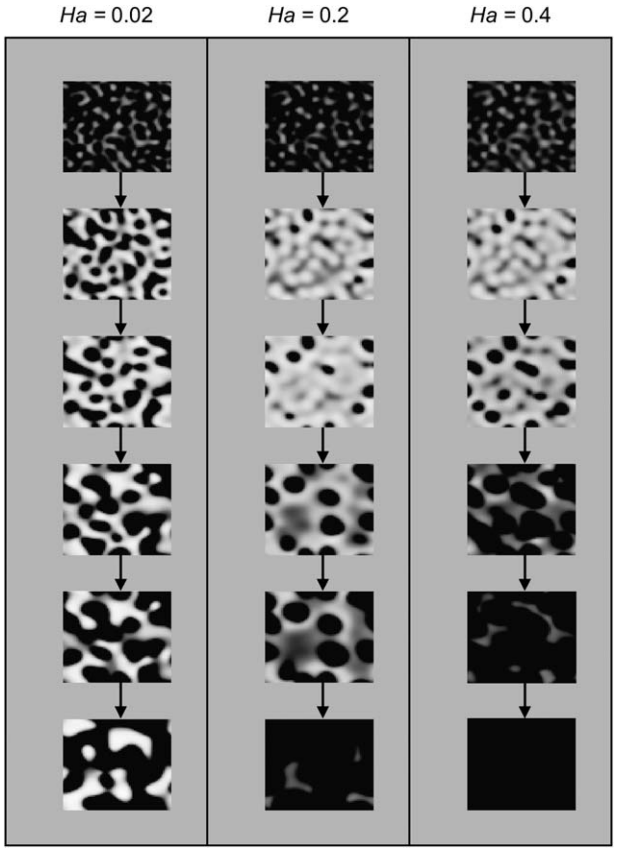

Fig. 8. Simulated pattern evolution of the parallel cross-section at $z = 12$ along z axis with different values of Ha. The time is 150, 500, 800, 1500, 2000 and 4000 from up to down.

Fig. 8 shows the evolution of the phase morphology at $z = 12$ with different values of Ha. The original conditions are the same. It is obvious that the evolutions of the phase morphology have almost the same change rule. Component A increases at the initial stage and the phase structure is from dispersed particle structure to the typical percolated phase structure. In the late stage, many holes, which become bigger gradually, appear. It can be found that the inversion of the phase structure appears during the separation with the fluctuation of the component concentration. The phase inversion is earlier as the increasing Ha. Furthermore, it is seen that t, the degree of the phase separation, increases with the increasing Ha. The phase structure at $Ha = 0.02$ is almost always the typical percolated phase structure in spite of the fluctuation of the component concentration.

Fig. 9 shows the evolution of the phase morphology in y direction with $y = 32$ and with different values of Ha, but the same original conditions. When the value of Ha is 0.2 and 0.4, the surface domain rapidly develops an enriched layer (in the preferred component, A) followed by a depleted layer. Next is another enriched layer, which has about the same average thickness as the enriched layer adjacent to the substrate. Farther from the substrate, the domain pattern has just the characteristic structure of bulk spinodal decomposition. The dynamics of phase separation in the vicinity of the substrate is enhanced because of the orientation effect of the

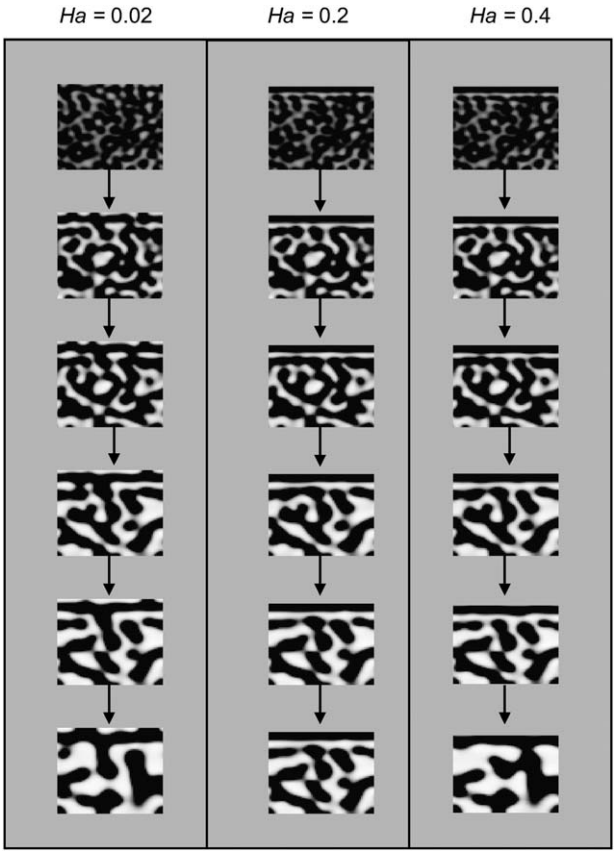

Fig. 9. Simulated pattern evolution of the perpendicular cross-section at $y = 32$ along y axis with different values of Ha. The time is 150, 500, 800, 1500, 2000 and 4000 from up to down.

surface layer which preferentially aligns domains parallel to the surface [32]. This results in anisotropy of domain growth parallel and perpendicular to the surface, in the vicinity of the surface. The degree of anisotropy decreases with increasing Z and the bulk is isotropic. It is also found that the degree of the phase separation increases with the increasing Ha. The wetting layer with $Ha = 0.4$ is thicker than that with $Ha = 0.2$ and, the substrate is only partially wetted with $Ha = 0.02$.

All the above results indicated that the higher surface potential of the substrate could enhance the degree and speed of the phase evolution. And the surface potential could result in the mutual transformation between completely wetting and partially wetting for the substrate interface.

3.4. Effects of the surface potential on the dynamical behavior

3.4.1. Dynamical behavior of the cross-section parallel to the substrate

In this section, we define the characteristic length scale of the pattern size based on the scattering function, $S(k,\tau)$. And the characteristic length $\langle k\rangle$ is defined as

$$\langle k\rangle = \frac{\int kS(k,\tau)\mathrm{d}k}{\int S(k,\tau)\mathrm{d}k} \tag{15}$$

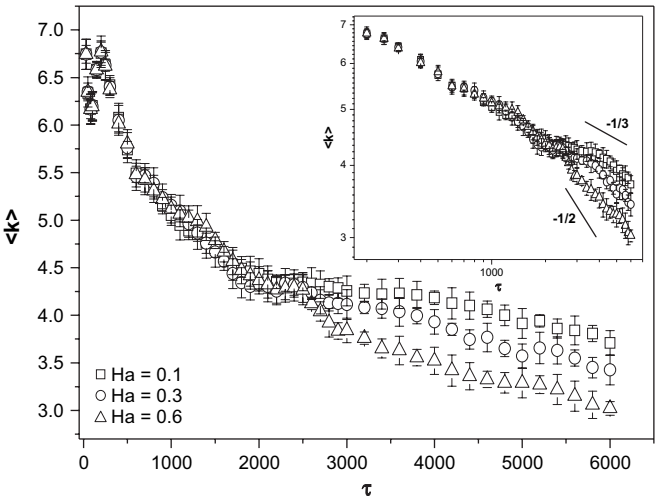

Fig. 10. Plots of $\langle k\rangle$ against time τ with $Ha = 0.1$, 0.3 and 0.6 at $Z = 22$. The inset shows the plots in the log–log scale.

Fig. 10 shows plots of $\langle k\rangle$ against time τ at $Z = 22$ with $Ha = 0.1$, 0.3 and 0.6. All results are averaged over 50 independent runs. It is found that the plots can be superposed in the early stage. However, these plots cross over at different times in the late stage, respectively. On the other hand, the length-scale data for different values of Ha evolves with almost the same speed initially and then cross over to a faster growth as the effect of the substrate is transported and inducted. The inset clarifies the crossover. Before the crossover, the growth law is $\langle k\rangle \propto \tau^{-1/3}$, demonstrating the typical LS growth law. Subsequent to the crossover, the accelerated growth seems to fit a faster law with about $\langle k\rangle \propto \tau^{-1/2}$ due to the orientation effect induced by the substrate [32]. The crossover is earlier for larger values of Ha, demonstrating that the higher the surface potential is, the faster the transmission speed of the effect from the substrate will be.

3.4.2. Dynamical behavior of the cross-section perpendicular to the substrate

We next consider the dynamical behavior of the cross-section perpendicular to the substrate by the real-space correlation function which can be defined as [25,26,32]

$$G(z1,z,\tau) = \langle\psi(x,y,z,\tau)\psi(x,y,z+z1,\tau)\rangle - \langle\psi(x,y,z,\tau)\rangle \times \langle\psi(x,y,z+z1,\tau)\rangle \tag{16}$$

The angular brackets refer to an averaging over initial conditions and integration over x and y. Furthermore, the characteristic length in the perpendicular direction, L, can be defined as

$$G(z+L,z,\tau) = G(0,z,\tau)/2 \tag{17}$$

where $G(0,z,\tau)$ is the maximum value of $G(z1,z,\tau)$.

Fig. 11 shows plots of $L(z,\tau)$ against τ at $Z = 22$ with $Ha = 0.1$, 0.3 and 0.6. And the inset is the plots in log–log scale. All results are averaged over 50 independent runs. It is seen that the perpendicular length scales follow the LS growth law until they experience the effect of the substrate

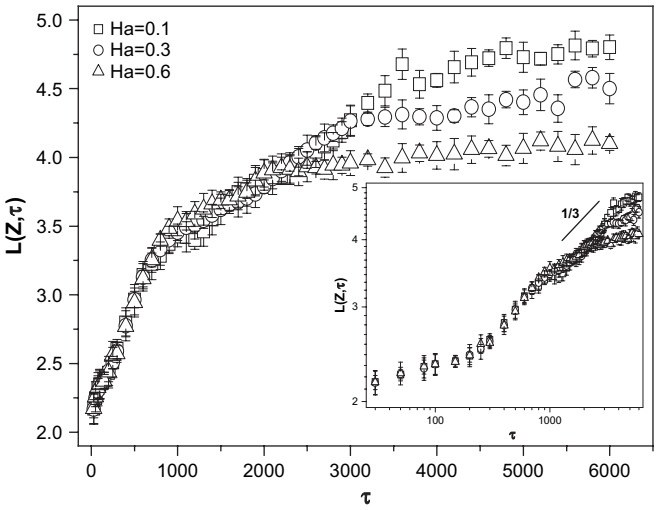

Fig. 11. Plots of $L(z,\tau)$ against τ with $Ha = 0.1$, 0.3 and 0.6 at $Z = 22$. The inset shows the plots in the log–log scale.

surface. In the late stage, the perpendicular length scale exhibits decelerated growth and even freezes at longer time. The freezing does not mean that there is no temporal evolution, but a dynamical equilibrium process [32]. It can also be found that the crossover is earlier for larger values of *Ha*, demonstrating that the higher surface potential leads to faster transmission speed of the effect of the substrate, corresponding to Fig. 10.

Moreover, it is interesting to know two basic factors. One is the character length which represents the distance from the wall where the effect of wall can be neglected. The other is the character time that oscillating profile near the substrate surface propagates to the character length during SDSD process. The results regarding these two basic factors may be helpful to gain insight into the dynamical behavior of SDSD, which will be discussed in detail in our next paper.

4. Conclusions

It is found that the thickness of the wetting layer, $R(\tau)$, increases with the increasing surface potential. A crossover, which is later for larger values of surface potential, appears in the evolution curve of $R(\tau)$. Before the crossover, the growth law is the surface potential dependant growth law. Subsequent to the crossover, the growth law is the typical LS growth law. These results are further proved by both the theoretical analysis of the current equation and the dynamical scaling of the rescaled averaged profiles. The results also show that $R(\tau)$ obeys the rule of $R(\tau) \propto Ha^{1/(\Theta+2)}$ in the early stage with the increasing values of the surface potential, however, in the late stage, $R(\tau)$ has no relation with *Ha*.

The results indicate that the higher surface potential of the substrate could enhance the degree and speed of the phase evolution. Moreover, the surface potential could result in the mutual transformation between completely wetting and partially wetting for the substrate interface. It is also found that higher surface potential leads to faster transmission of the effect of the substrate.

Acknowledgments

Financial support from the National Natural Science Foundation of China (Nos. 50573088, 90103035, 20174022 and 10334020) and the Specialized Research Fund for the Doctoral Program of Higher Education (No. 20040003033) is highly appreciated.

References

[1] Puri S. J Phys Condens Matter 2005;17:R101–42 [and references therein].
[2] Geoghegan M, Krausch G. Prog Polym Sci 2003;28:261–302 [and references therein].
[3] Jones RAL, Norton LJ, Kramer EJ, Bates FS, Wiltzius P. Phys Rev Lett 1991;66:1326–9.
[4] Guenoun P, Beysens D, Robert M. Physica A 1991;172:137–40.
[5] Wang W, Shiwaku T, Hashimoto T. Macromolecules 2003;36:8088–96.
[6] Nakai A, Shiwaku T, Wang W, Hasegawa H, Hashimoto T. Macromolecules 1996;29:5990–6001.
[7] Sung L, Karim A, Douglas JF, Han CC. Phys Rev Lett 1996;76:4368–71.
[8] Geoghegan M, Jones RAL, Clough AS. J Chem Phys 1995;103:2719–24.
[9] Geoghegan M, Ermer H, Jüngst G, Krausch G, Brenn R. Phys Rev E 2000;62:940–50.
[10] Karim A, Douglas JF, Lee BP, Glotzer SC, Rogers JA, Jackman RJ, et al. Phys Rev E 1998;57:R6273–6.
[11] Böltau M, Walheim S, Mlynek J, Krausch G, Steiner U. Nature 1998;391:877–9.
[12] Kargupta K, Sharma A. Phys Rev Lett 2001;86:4536–9.
[13] Kargupta K, Sharma A. Langmuir 2002;18:1893–903.
[14] Krausch G, Dai C-A, Kramer EJ, Bates FS. Phys Rev Lett 1993;71:3669–72.
[15] Xie X-M, Xiao T-J, Zhang Z-M. J Colloid Interface Sci 1998;206:189–94.
[16] Xie X-M, Kong X-M, Xiao T-J, Yang Y, Gao N, Tanioka A. J Colloid Interface Sci 2001;234:24–7.
[17] Xie X-M, Chen Y, Zhang Z-M, Tanioka A, Matsuoka M, Takemura K. Macromolecules 1999;32:4424–9.
[18] Zong Q, Li Z, Xie X-M. Macromol Chem Phys 2004;205:1116–24.
[19] Liu YD, Kong X-M, Xie X-M. Acta Polym Sin 2002;6:824–7.
[20] Straub W, Bruder F, Brenn R, Krausch G, Bielefeldtm H, Krisch A, et al. Europhys Lett 1995;29:353–61.
[21] Wiltzius P, Cumming A. Phys Rev Lett 1991;66:3000–3.
[22] Cumming A, Wiltzius P, Bates FS, Rosedale JH. Phys Rev A 1992;45:885–97.
[23] Krausch G, Mlynek J, Straub W, Brenn R, Marko JF. Europhys Lett 1994;28:323–9.
[24] Puri S, Binder K. Phys Rev A 1992;46:R4487–9.
[25] Puri S, Binder K. Phys Rev E 1994;49:5359–77.
[26] Puri S, Binder K. Phys Rev E 1997;56:6991–7000.
[27] Puri S, Binder K. Phys Rev Lett 2001;86:1797–800.
[28] Puri S, Binder K. Phys Rev E 2002;66:061602.
[29] Lee BP, Douglas JF, Glotzer SC. Phys Rev E 1999;60:5812–22.
[30] Marko JF. Phys Rev E 1993;48:2861–79.
[31] Kuksenok O, Balazs AC. Phys Rev E 2003;68:011502.
[32] Yan L-T, Xie X-M. Polymer 2005;46:7684–94.
[33] Binder K, Frisch HL. Phys B 1991;84:403–9.
[34] Sagui C, Somoza AM, Roland C, Desai RC. J Phys A Math Gen 1993;26:L1163–8.
[35] Rysz J. Polymer 2005;46:977–82.
[36] Yan L-T, Xie X-M. Macromolecules 2006;39:2388–97.

[37] Ginzburg VV, Qiu F, Balazs AC. Polymer 2002;43:461–6.
[38] Feng J, Ruckenstein E. Polymer 2002;43:5775–90.
[39] Gestoso P, Brisson J. Polymer 2003;44:7765–76.
[40] Lam Y-M, Goldbeck-Wood G. Polymer 2003;44:3593–605.
[41] Gunton JD, San Miguel M, Sahni PS. Phase transitions and critical phenomena. In: Domb C, Lebowitz J, editors. London: Academic Press; 1990.
[42] Ohata T, Enomoto Y, Harden JL, Doi M. Macromolecules 1993;26: 4928–34.
[43] de Gennes PG. Rev Mod Phys 1985;57:827–63.
[44] Luo K, Yang Y. Macromolecules 2002;35:3722–30.
[45] Luo K, Yang Y. Polymer 2004;45:6745–51.
[46] Yan L-T, Xie X-M. Macromol Theor Simul 2006;15:226–37.
[47] Oono Y, Puri S. Phys Rev A 1988;38:434–53.
[48] Puri S, Oono Y. Phys Rev A 1988;38:1542–65.
[49] Lifshitz IM, Slyozov VV. J Phys Chem Solids 1961;35:19–25.
[50] Onuki A. Phase transition dynamics. London: Cambridge University Press; 2002.
[51] Bray AJ. Adv Phys 1994;43:357–459.
[52] Brown G, Chacrabarti A. Phys Rev A 1992;46:4829–35.